Stride-to-stride energy regulation for robust self-stability of a torque-actuated dissipative spring-mass hopper

M. Mert Ankarali, and Uluç Saranli

View Online   Export Citation

ARTICLES YOU MAY BE INTERESTED IN

Stride-to-stride energy regulation for robust self-stability of a torque-actuated dissipative spring-mass hopper

M. Mert Ankarali[1,a)] and Uluç Saranli[2,b)]

[1]*Department of Electrical and Electronics Engineering, Middle East Technical University, 06531 Ankara, Turkey*
[2]*Department of Computer Engineering, Bilkent University, 06800 Ankara, Turkey*

In this paper, we analyze the self-stability properties of planar running with a dissipative spring-mass model driven by torque actuation at the hip. We first show that a two-dimensional, approximate analytic return map for uncontrolled locomotion with this system under a fixed touchdown leg angle policy and an open-loop ramp torque profile exhibits only marginal self-stability that does not always persist for the exact system. We then propose a per-stride feedback strategy for the hip torque that explicitly compensates for damping losses, reducing the return map to a single dimension and substantially improving the robust stability of fixed points. Subsequent presentation of simulation evidence establishes that the predictions of this approximate model are consistent with the behavior of the exact plant model. We illustrate the relevance and utility of our model both through the qualitative correspondence of its predictions to biological data as well as its use in the design of a task-level running controller. © *2010 American Institute of Physics.*
[doi:10.1063/1.3486803]

It has long been established that simple spring-mass systems, such as the well-studied spring-loaded inverted pendulum (SLIP) model, can accurately represent the dynamics of legged locomotion. However, the existing work in this domain almost exclusively focuses on lossless leg models with actuation through tunable leg stiffness, making it difficult to generalize associated results to physical systems. In this paper, we introduce a more realistic model with damping and actuation through a controllable hip torque, subsequently developing a sufficiently accurate analytic approximation to identify and characterize its limit cycles. We show that in the absence of any explicit controls, running with this model is only marginally stable, but when an "energy regulating" feedback law is introduced on the stance hip torque, an open-loop, fixed touchdown angle policy produces asymptotically stable running across a much larger range of states. We also show that the relatively understudied hip torque actuation not only provides robust stability properties, but also has interesting correspondence to data from biological runners, more accurately predicting horizontal ground reaction forces during locomotion.

I. INTRODUCTION

Long term practical utility of mobile robots in unstructured environments critically depends on their locomotory aptitude. In this context, the performance of ground mobility that can ultimately be achieved by legged platforms is superior to any other alternative as evidenced by numerous examples in nature as well as a number of very successful dynamically stable autonomous legged robots that have been built to date.[1–5] Unfortunately, even on flat ground, legged morphologies do not enjoy the simplicity of models supported by the conveniently constrained and continuous modes of ground interaction observed in wheeled and, to some extent, tracked vehicles. Even the most basic legged behaviors such as walking[6–10] and running[11] require hybrid dynamic models whose analysis and control involve difficult challenges. In the world of quasistatic locomotion with multilegged robots, one can recover some of this simplicity through active or structural suppression of second-order dynamics,[12] but these methods are not directly applicable to dynamically dexterous modes of locomotion such as running.

One of the most significant discoveries in this context was most likely the recognition of similar center-of-mass (COM) movement patterns in running animals of widely different sizes and morphologies.[13–17] This led to the development of the simple yet accurate SLIP model to describe such behaviors.[18,19] Significant research effort was devoted to both the use of this model as a basis for the design of fast and efficient legged robots[1,2,20,21] and associated control strategies[22,23] as well as its analysis to reveal fundamental aspects of legged locomotory behaviors.[11] The present paper falls into the latter category and contributes by investigating the previously unaddressed question of how the presence of passive damping and actuation through a controllable hip torque affects the behavioral characteristics of running. Our approach is based on recently proposed analytic approximations to the dynamics of a dissipative SLIP model,[24] which can capture the effects of viscous damping in the leg much more accurately than previously available methods in the literature that rely on the conservation of energy.[25–28] Since

a)Electronic mail: ankarali@eee.metu.edu.tr.
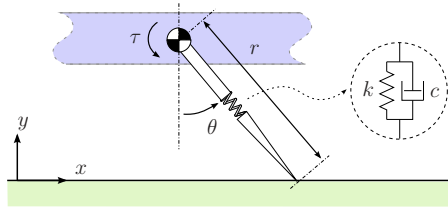b)Electronic mail: saranli@cs.bilkent.edu.tr.

FIG. 1. (Color online) TD-SLIP: planar, dissipative spring-mass hopper with rotary hip actuation.

FIG. 2. (Color online) A single TD-SLIP stride with definitions of transition states. The (cyclic) horizontal position variable at apex x_a and the fixed leg length at touchdown $r_{td}=r_0$ are omitted for simplicity.

trajectories of this dissipative model lack symmetry properties necessary to indirectly deduce stability properties without an explicit return map,[29,30] we use our analytic approximations to generalize previous uses of Poincaré methods[26,31–34] to the stability analysis of running with a dissipative spring-mass model.

Our contributions in the present paper have a number of important differences from existing work. First, our plant model is dissipative, invalidating most existing analytic approximations and their predictions. Second, in contrast to the usual energy-regulation mechanisms in the literature through adjustments of the leg length or changing stiffness, our model uses only a single torque actuator at the hip to compensate for energy losses. These differences are motivated by being much more realistic from an implementation point of view, as evidenced by the successful use of similar actuation mechanisms in a number of monopedal platforms,[35,36] the Scout quadrupeds,[5] as well as the RHex hexapod.[1] Finally, our approximate solutions to the return map also take into account the effect of gravity on the angular momentum for steps that are nonsymmetric with respect to the gravitational vertical, increasing the practical applicability of our stability results.

II. THE TORQUE-ACTUATED DISSIPATIVE SLIP MODEL

A. System dynamics and the apex return map

Figure 1 illustrates the torque-actuated dissipative spring-loaded inverted pendulum (TD-SLIP) plant we investigate in this paper. It consists of a fixed orientation (2 degrees-of-freedom) planar rigid body with mass m, connected to a massless, fully passive leg with linear compliance k, rest length r_0, and linear viscous damping c, through an actuated rotary joint with torque τ. Section II B provides detailed justifications for our choice of fixed body orientation within this model.

The TD-SLIP system alternates between *stance* and *flight* phases during running, with the flight phase further divided into the *ascent* and *descent* subphases. Figure 2 illustrates three important events that define transitions between these phases: *touchdown*, where the leg comes into contact with the ground, *liftoff*, where the toe takes off from the ground, and finally *apex*, where the body reaches its maximum height during flight with $\dot{y}=0$. Another important event, not illustrated in the figure, is *bottom*, where the leg is maximally compressed during stance. Table I details the notation used throughout the paper.
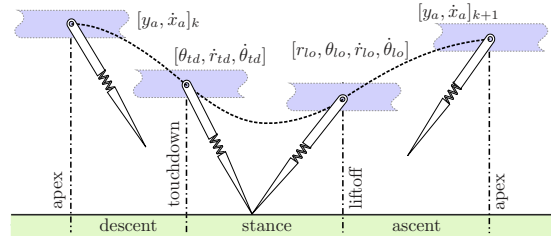
During flight, the body obeys ballistic flight dynamics,

$$\begin{bmatrix} \ddot{x} \\ \ddot{y} \end{bmatrix} = \begin{bmatrix} 0 \\ -g \end{bmatrix}, \tag{1}$$

and the massless leg can be arbitrarily positioned. In contrast, during stance, the toe remains stationary on the ground while the body mass feels forces generated by both the passive spring-damper pair and the hip torque. The exact stance dynamics of the SLIP model in polar leg coordinates with respect to the toe location take the form

$$\frac{d}{dt}\begin{bmatrix} m\dot{r} \\ mr^2\dot{\theta} \end{bmatrix} = \begin{bmatrix} mr\dot{\theta}^2 - mg\cos\theta - k(r-r_0) - c\dot{r} \\ mgr\sin\theta + \tau \end{bmatrix}, \tag{2}$$

easily derived using a Euler–Lagrange formulation.

A very useful abstraction for the analysis and control of cyclic TD-SLIP trajectories is provided by the apex return map, induced by the Poincaré section $\dot{y}=0$ during flight. In Secs. III and IV, we will use this map to study the stability properties of TD-SLIP, and later adopt it in Sec. V as a task-level gait representation for a closed-loop running controller.

We will find it convenient to define three individual submaps,

$$P_d:[y_a,\dot{x}_a] \rightarrow [\dot{r}_{td}, \dot{\theta}_{td}], \tag{3}$$

$$P_s:[\dot{r}_{td}, \dot{\theta}_{td}] \rightarrow [r_{lo}, \theta_{lo}, \dot{r}_{lo}, \dot{\theta}_{lo}], \tag{4}$$

TABLE I. Notation used throughout the paper.

| System states, event states, and control inputs	
$x, y, \dot{x}, \dot{y}$	Cartesian body position and velocities
$r, \theta, \dot{r}, \dot{\theta}$	Leg length, leg angle, and velocities
τ	Hip torque command during stance
$y_a, \dot{x}_a$	Apex height and velocity
E_a	Apex energy
$\theta_{td}, \dot{r}_{td}, \dot{\theta}_{td}$	Touchdown leg angle, polar velocities
t_b, r_b, θ_b	Bottom time, leg length, and angle
$t_{lo}, r_{lo}, \theta_{lo}, \dot{r}_{lo}, \dot{\theta}_{lo}$	Liftoff time, leg length, angle, and velocities
p_θ	Angular momentum around the toe
Kinematic and dynamic parameters	
m, g	Body mass and gravitational acceleration
k, r_0, c	Leg stiffness, rest length, and damping
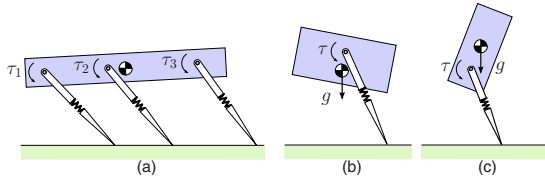
FIG. 3. (Color online) Possible robot morphologies for which the TD-SLIP model is relevant. (a) A planar hexapod with individually actuated hips. (b) A monopedal platform with low center of mass. (c) A human-like morphology with an upright body posture.

$$P_a:[r_{lo}, \theta_{lo}, \dot{r}_{lo}, \dot{\theta}_{lo}] \rightarrow [y_a, \dot{x}_a], \qquad (5)$$

for the descent, stance, and ascent phases, respectively, to yield the overall apex return map as $P := P_a \circ P_s \circ P_d$. Note that the liftoff states incorporate additional redundant variables for convenience, but the apex return map is two-dimensional. The descent and ascent maps are trivial and are given by

$$P_d: \begin{bmatrix} \dot{r}_{td} \\ r_0 \dot{\theta}_{td} \end{bmatrix} = -R(\pi/2 - \theta_{td}) \begin{bmatrix} \dot{x}_a \\ -\sqrt{2g(y_a - r_0 \cos \theta_{td})} \end{bmatrix}, \qquad (6)$$

$$P_a: \begin{bmatrix} y_a \\ \dot{x}_a \end{bmatrix} = \begin{bmatrix} r_{lo} \cos \theta_{lo} + \dot{y}_{lo}^2/(2g) \\ \dot{x}_{lo} \end{bmatrix}, \qquad (7)$$

where $\dot{x}_{lo}$ and $\dot{y}_{lo}$ are liftoff velocities in Cartesian coordinates and R denotes the standard two-dimensional rotation matrix. Unfortunately, the stance dynamics of Eq. (2) are not integrable in closed form. In Sec. II C, we briefly review the analytical approximations to the stance dynamics of a dissipative SLIP model proposed by Ankarali *et al.*,[24] and extend it in Sec. II D to support hip torque actuation.

B. Relevance and feasibility of hip torque actuation

The TD-SLIP model described above assumes a fixed body orientation that enables controllable torque actuation at the hip, while also being sufficiently simple to admit the approximate analytical solutions we present in Secs. II C and II D. Even though this assumption seems to be rather unrealistic for an actual legged machine, it should be noted that our model is not intended for direct realization on a legged platform, just as the original SLIP model with its point-mass riding on a compliant leg did not directly correspond to any physical animal or robot morphology.[11] Our main motivation is to gain a focused understanding of stability properties in the presence of attributes common to a large range of legged morphologies, passive damping, and hip torque actuation in particular, within a model sufficiently descriptive but simple enough to provide analytical insight.

Nevertheless, practical relevance and applicability of this model to physical systems also need to be established. In this section, we briefly describe three different, physically plausible morphologies (or "anchors"[37]) illustrated in Fig. 3 that would benefit from using TD-SLIP as the underlying "template" to analyze and control their locomotory performance. It should be noted that detailed analysis of these

models is beyond the scope of the present paper, so we only provide sufficient detail to establish the applicability of our model.

Figure 3(a) shows a simplified planar model of the RHex hexapod[1] which incorporates three torque actuated, passively compliant legs, each representing a contralateral pair of physical legs. The body angle is not explicitly constrained, but the front and back legs provide restoring forces that passively push the body angle toward the horizontal. Moreover, we have recently shown that active, template-based control can also use hip torques to actively regulate the body angle, while simultaneously controlling the locomotory center-of-mass dynamics.[38] In contrast to our previous use of the passive SLIP model, TD-SLIP would be a much better template with which this hexapedal robot can be analyzed and controlled.

In contrast, Fig. 3(b) shows a monopedal platform where the leg is attached above the center of mass to exploit the stability of natural pendulum dynamics. This is a principle that has been used by most successful monopod robots with a freely rotating body.[39,40] In our case, the restoring torque provided by gravity would passively counteract the leg torque, making it possible to approximately embed TD-SLIP dynamics within this more complex morphology. Further research is of course needed to establish that perturbations arising from body oscillations do not destroy TD-SLIP stability, but we think this is one of the simpler ways in which our results can be applied to physical robots.

Finally, Fig. 3(c) illustrates a human-like legged morphology with an upright body posture,[23] the most difficult scenario for which the TD-SLIP morphology would be relevant. Unlike the previous example, body dynamics are close to those of an inverted pendulum and are naturally unstable. Nevertheless, we believe that it would still be possible to use a properly chosen body angle trajectory that would both allow an approximate realization of the hip torque profile required by our analysis in Sec. II D, while also stabilizing around a body angle trajectory that would provide the necessary gravitational torque to counteract the hip torque. This idea is similar in spirit to the extension of passive dynamic walking models[6] to incorporate an upright torso[41,42] both for energy input and balance.

Now that we have provided a context for the utility of the TD-SLIP model, we proceed with a detailed analysis of and approximate solutions of its dynamics.

C. Approximate stance map for the unforced TD-SLIP

Similar to earlier work on conservative SLIP models,[26] approximations to the stance trajectories of a dissipative SLIP model proposed by Ankarali *et al.*[24] rely on two key assumptions: (1) the angular travel throughout the stance is relatively small and remains close to the vertical, allowing linearization of the gravitational potential in the Lagrangian with subsequent conservation of the angular momentum $p_\theta := mr^2\dot{\theta}$ and (2) the radial compression is small with $r_0 - r \ll r_0$, allowing a truncated Taylor expansion of related terms. Even though these assumptions seem rather limiting, we found that the resulting approximate return map remains

accurate for leg compressions up to 75% of the spring rest length as well as deviations of up to 30° away from the vertical using our gravity correction method of Sec. II D. Under these conditions and assuming, for now, that $\tau = 0$, the radial component of Eq. (2) reduces to

$$\ddot{r} + (c/m)\dot{r} + (\omega_0^2 + 3\omega^2)r = -g + r_0\omega_0^2 + 4r_0\omega^2, \quad (8)$$

with the definitions $\omega_0 := \sqrt{k/m}$ and $\omega := p_\theta/(mr_0^2)$. Solutions to this simple second-order ordinary differential equation can be found as

$$r(t) = e^{-\zeta\hat{\omega}_0 t}(A\cos(\omega_d t) + B\sin(\omega_d t)) + F/\hat{\omega}_0^2, \quad (9)$$

with $\hat{\omega}_0 := \sqrt{\omega_0^2 + 3\omega^2}$, $\zeta := c/(2m\hat{\omega}_0)$, $\omega_d := \hat{\omega}_0\sqrt{1-\zeta^2}$, and $F := -g + r_0\omega_0^2 + 4r_0\omega^2$. A and B are determined by touchdown states as

$$A := r_0 - F/\hat{\omega}_0^2, \quad (10)$$

$$B := (\dot{r}_{td} + \zeta\hat{\omega}_0 A)/\omega_d. \quad (11)$$

Simple differentiation and further simplification yield radial TD-SLIP trajectories as

$$r(t) = Me^{-\zeta\hat{\omega}_0 t}\cos(\omega_d t + \phi_1) + F/\hat{\omega}_0^2, \quad (12)$$

$$\dot{r}(t) = -M\hat{\omega}_0 e^{-\zeta\hat{\omega}_0 t}\cos(\omega_d t + \phi_1 + \phi_2), \quad (13)$$

with $M := \sqrt{A^2 + B^2}$, $\phi_1 := \arctan(-B/A)$, and $\phi_2 := \arctan(-\sqrt{1-\zeta^2}/\zeta)$. At this point, the angular trajectories can be determined using the constant angular momentum. An additional linearization of the term $1/r^2$ in the angular momentum leads to an analytical solution for the rate of change of the leg angle as

$$\dot{\theta}(t) = 3\omega - 2\omega F/(r_0\hat{\omega}_0^2) - 2\omega Me^{-\zeta\hat{\omega}_0 t}\cos(\omega_d t + \phi_1)/r_0, \quad (14)$$

integrated to yield the angular trajectory

$$\theta(t) = \theta_{td} + Xt + Y(e^{-\zeta\hat{\omega}_0 t}\cos(\omega_d t + \phi_1 - \phi_2) - \cos(\phi_1 - \phi_2)), \quad (15)$$

with $X := 3\omega - 2\omega F/(r_0\hat{\omega}_0^2)$ and $Y := 2\omega M/(r_0\hat{\omega}_0)$ defined accordingly.[24]

The final step in completing the stance map requires finding the time of liftoff. Since we do not allow explicit control of the liftoff leg length, only the force based liftoff condition[24] is applicable in the context of the present paper. Consequently, the liftoff time is solely determined by vanishing point of the spring-damper force felt by the toe with $k(r_0 - r(t_{lo})) - c\dot{r}(t_{lo}) = 0$, for which a sufficiently accurate analytical approximation can be found by noting that the compression and decompression times are often roughly equal with $e^{-\zeta\hat{\omega}_0 t_{lo}} \approx e^{-\zeta\hat{\omega}_0 2t_b}$, where t_b denotes the *bottom time*, easily found by solving Eq. (13). This assumption, of course, introduces inaccuracies since stance trajectories for the damped spring are not symmetric with decompression times often slightly longer than compression times. However, since we only approximate the exponential term in Eq. (13), we still obtain a sufficiently good approximation while maintaining conceptual simplicity. We now have

$$t_{lo} \approx (2\pi - \arccos(k(r_0 - F/\hat{\omega}_0^2)/(\bar{M}Me^{-\zeta\hat{\omega}_0 2t_b})) - \phi_1 - \phi_3)/\omega_d, \quad (16)$$

with $\bar{M} := \sqrt{k^2 - 2kc\hat{\omega}_0\cos\phi_2 + c^2\hat{\omega}_0^2}$ and $\phi_3 := \arctan((c\hat{\omega}_0\sin\phi_2)/(c\hat{\omega}_0\cos\phi_2 - k))$, resulting in the stance map

$$P_s: \begin{bmatrix} r_{lo} \\ \theta_{lo} \\ \dot{r}_{lo} \\ \dot{\theta}_{lo} \end{bmatrix} = \begin{bmatrix} r(t_{lo}) \\ \theta(t_{lo}) \\ \dot{r}(t_{lo}) \\ \dot{\theta}(t_{lo}) \end{bmatrix}, \quad (17)$$

where the right hand side is a function of touchdown states.

Note, however, that the derivations of Ankarali *et al.*[24] that we summarized above ignore the presence of the hip torque. In Sec. II D, we propose a new method to incorporate the effects of both the hip torque and gravity through a fixed correction[28] on the angular momentum value p_θ.

D. Approximate stance map for the forced TD-SLIP

Hip actuation in legged systems can serve a number of different purposes. Among both biological[17] and robotic[20,21,43,44] systems, its most common uses involve retraction of legs in flight and control of body posture with legs in stance. Interestingly, the use of hip actuation to provide thrust has not been studied as extensively in the robotics literature. In addition to a few direct experimental inquiries[35,36] and indirect uses in multilegged platforms,[1,5,45] it has received limited attention in the form of an active spring.[30] Recent research also indicates that quadrupedal locomotion uses forward thrust through the use of hip actuators to provide an impulsive energy source.[46]

Our use of the hip torque as a means of energy input instead of radial actuation strategies such as tunable springs[47] or toe push-off prior to liftoff is primarily motivated by the ease of incorporating hip actuators within physical robot platforms.[1,5] Even though radial actuation alternatives have been shown to provide better efficiency for passive dynamic walking behaviors due to their ability to minimize impact losses,[48] similar benefits do not carry over to legs with compliance where impact losses are less pronounced. Consequently, in the present paper, we propose an open-loop hip actuation regime that enforces the ramp torque profile,

$$\tau(t) = \begin{cases} \tau_0\left(1 - \dfrac{t}{t_f}\right) & \text{if } 0 \le t \le t_f \\ 0 & \text{if } t > t_f, \end{cases} \quad (18)$$

during stance, with τ_0 and t_f chosen prior to touchdown. This open-loop profile has three important advantages. First, its simple functional dependence on time allows us to easily incorporate its effects into the derivations of Sec. II C. Second, if we choose t_f to be the predicted liftoff time, we have $\tau(t_{lo}) = 0$, which prevents premature leg liftoff due to the action of the hip and ensures a structural match to the trajectories of the unforced system. Such a match is not possible with the constant hip torque profiles adopted by earlier work. Finally, the unidirectional action of our ramp torque profile

ensures that no negative work is done during stance, ensuring locomotion efficiency. Since, by definition, the limit cycles we study in Secs. III and IV require zero net change in the total system energy and hence always correspond to positive energy input from the hip torque, our avoidance of negative work will not have any impact on our stability results.

Inspection of the TD-SLIP dynamics of Eq. (2) shows that the hip torque directly acts on the angular dynamics and only indirectly affects radial motion. Consequently, we hypothesize that an average correction to the constant angular momentum p_θ of Sec. II C can capture the effects of the hip torque on system trajectories. Normally, the instantaneous angular momentum around the toe during stance can be formulated as

$$p_\theta(t) = p_\theta(0) + \int_0^t \tau(\eta) d\eta + \int_0^t mgr(\eta)\sin\theta(\eta) d\eta, \quad (19)$$

by direct integration of the angular dynamics. Similar to previous work on gravity correction,[28] we compute a corrected angular momentum,

$$\hat{p}_\theta = p_\theta(0) + \Delta p_\tau + \Delta p_g, \quad (20)$$

where Δp_τ and Δp_g incorporate the time averaged effects of the leg torque and gravitational acceleration, respectively. Fortunately, our choice of the ramp torque profile admits a very simple analytic solution for Δp_τ. Assuming $t_f = t_{lo}$ in Eq. (18), we have

$$\Delta p_\tau := \frac{1}{t_{lo}} \int_0^{t_{lo}} \left(\int_0^{\eta_1} \tau(\eta_2) d\eta_2 \right) d\eta_1 = \tau_0 \frac{t_{lo}}{3}. \quad (21)$$

However, even with available analytic approximations, derivation of an exact closed-form expression for Δp_g is not feasible. Instead, we use a linear approximation to the integrand $r(\eta)\sin\theta(\eta)$ using its values at the touchdown and liftoff, resulting in

$$\Delta p_g := \frac{mgt_{lo}}{6}(2r_0 \sin\theta_{td} + r_{lo}\sin\theta_{lo}). \quad (22)$$

Estimated values for the liftoff time t_{lo}, leg angle θ_{lo}, and leg length r_{lo} are provided by the unforced approximations of Sec. II C. Substituting $\hat{p}_\theta$ for the constant angular momentum in all derivations of Sec II C, we obtain a new approximation that takes into account the effects of both the hip torque and gravity on the stance trajectories.

Note that the corrections we propose have an iterative character since both Eqs. (21) and (22) use prior estimates of t_{lo} and θ_{lo}. Consequently, starting from the unforced approximations, it is possible to iteratively apply these corrections to obtain more accurate predictions at the expense of analytic simplicity. Currently, we do not have a global convergence proof similar to previous iterative maps for conservative SLIP models,[19] but our simulations have shown convergence for all but the most extreme initial conditions such as the angle of attack being very close to the touchdown leg angle, causing a bounce-back. In any case, a single iteration usually yields sufficiently accurate results for our purposes and we do not rely on the iterative character of our approximations for the rest of the present paper.

III. STABILITY OF UNCONTROLLED TD-SLIP LOCOMOTION

The biological origins of the SLIP model primarily support its *descriptive* power for center-of-mass movements of running animals.[19] However, despite all the evidence indicating a close match between steady-state trajectories generated by the SLIP model and those arising from the complex neuromechanics of running animals,[11] it is much less clear whether this correspondence generalizes to transient behavior and how well this model can predict stability properties and modes of control associated with running behaviors. This is a rather broad question that requires a much deeper understanding of both musculoskeletal and neural mechanisms involved in running animals than what is currently known. Nevertheless, the study of inherent, open-loop stability properties associated with locomotory models can provide both evidence toward possible reasons behind their adoption by biological runners as well as hypotheses which can be explicitly verified by biomechanical experiments.[49] Previous investigations of SLIP self-stability exclusively rely on conservation of energy and the resulting one-dimensional return map once energy and the cyclic horizontal position variables are factored out.[26,50–52] For the TD-SLIP model, however, energy is not necessarily conserved from one apex to the next, necessitating the study of a two-dimensional return map. In this section, we describe a method to effectively isolate fixed points of this return map and subsequently characterize their stability by means of an analytically formulated Jacobian.

A. Equilibrium points of the uncontrolled return map

Recall that our choice of the hip torque in Eq. (18) incorporates two parameters: τ_0 and t_f. We have already observed that choosing $t_f = t_{lo}$ is advantageous in preventing early liftoff and ensuring structural correspondence of system trajectories to our analytical approximation, leaving only τ_0 to be determined for a fully specified return map. Earlier studies of vertically constrained hopping revealed that the combination of constant energy input with viscous damping in the leg yields global, asymptotic stability as a result of the associated unimodal return map.[18] Following a similar line of inquiry, we find it most convenient to work in a new set of coordinates, the apex height, and the total mechanical energy, yielding a new return map definition, a simple coordinate change away from the map described in Sec. II C as

$$\begin{bmatrix} y_a[k+1] \\ E_a[k+1] \end{bmatrix} = \tilde{P}\left(\begin{bmatrix} y_a[k] \\ E_a[k] \end{bmatrix} \right). \quad (23)$$

We have excluded the cyclic horizontal position variable from this map since forward locomotion is expected to be periodic in only the remaining variables. In the rest of this section, we will study the stability properties of this map under an *open-loop* strategy, with a constant touchdown angle $\theta_{td} = \beta$ and a fixed hip torque during stance for each stride. For more general applicability, all of our numerical results will be presented in nondimensional coordinates, defined as
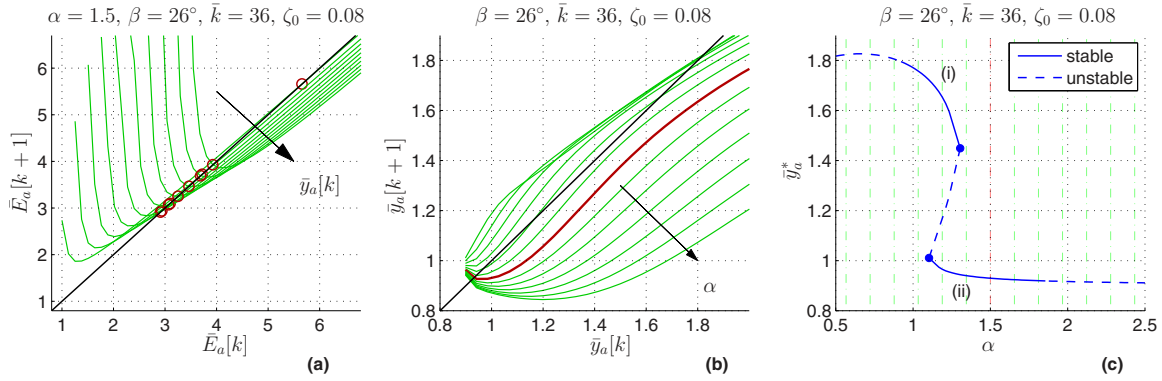
FIG. 4. (Color online) (a) Cross sections of the two-dimensional TD-SLIP return map along the energy axis for $\alpha=1.5$ and $\beta=26°$ plotted for different apex height values $\bar{y}_a[k]$. (b) Cross sections of the return map constrained to energy solutions of Eq. (27) plotted for different values of α. The middle thick curve corresponds to the locus of the energy fixed points marked with circles in the left plot. (c) Fixed points of the apex height in the middle figure as a function of α. All axes are shown in dimensionless units as defined in Eq. (24).

$$\bar{y}_a := y_a/r_0, \quad \bar{\dot{x}}_a := \dot{x}_a/\sqrt{gr_0},$$

$$\bar{E}_a := E_a/(mgr_0), \quad \bar{k} := kr_0/(mg), \qquad (24)$$

$$\zeta_0 := c/(2\sqrt{mk}), \quad \bar{\tau} := \tau/(mgr_0).$$

Moreover, to make comparisons with earlier studies easier, we use kinematic and dynamic parameters that roughly match those of an average human with $m=80$ kg and $r_0=1$ m.

For the TD-SLIP system, the energy supplied by the hip during stance is given by

$$E_\tau = \tau_0 \int_0^{t_{lo}} \left(1 - \frac{t}{t_{lo}}\right) \dot{\theta}(t) dt. \qquad (25)$$

The closest correspondence to Raibert's runners[20] and the analysis of Koditschek and Buehler[18] would have been obtained if we were to use our approximations of Sec. II D to obtain closed-form expressions for this energy input and solve for τ_0 that would have yielded a fixed energy input at every stride. Intuitively, since damping losses monotonically increase with the total energy level of the system, this constant energy input is likely to stabilize the system around a fixed energy level. However, in order to isolate self-stability properties of the uncontrolled TD-SLIP model, we use a much simpler, open-loop strategy for the hip torque during stance with

$$\tau_0 = \frac{C}{\dot{\theta}_{td}}, \qquad (26)$$

where C is an independent parameter with its dimensionless counterpart defined as $\alpha := C/(mg\sqrt{gr_0})$ and $\dot{\theta}_{td}$ is the angular velocity at touchdown, easily computed using ballistic flight trajectories. This choice corresponds to a fixed power at touchdown, and roughly approximates constant energy input during stance, resulting in a unimodal structure for the energy component of the apex return map, as shown in Fig. 4(a). In order to locate the fixed points of the return map $\widetilde{P}$, we first find apex energy levels E_a^* that are preserved by

this return map for a given height as the solutions to the equation,

$$[y_a[k+1], E_a^*] = \widetilde{P}([y_a[k], E_a^*]). \qquad (27)$$

As a result of the unimodal structure of the energy return map, this always yields a single solution. The resulting constrained energy surface allows us to define a one-dimensional cross section of the return map for the apex height, whose zeroes correspond to the fixed points of $\widetilde{P}$, as shown in Fig. 4(b) for different values of α. More formally, we define the apex height values preserved by the return map y_a^* as solutions to the equation,

$$[y_a^*, E_a^*(y_a^*)] = \widetilde{P}([y_a^*, E_a^*(y_a^*)]), \qquad (28)$$

which is one-dimensional and easily solved numerically to identify all fixed points $[y_a^*, E_a^*]$ of the two-dimensional apex return map $\widetilde{P}$. Note that we have slightly abused notation with $E_a^*(y_a^*)$, which is not a function because it has multiple values corresponding to multiple fixed points at a given apex height. However, it is still straightforward to numerically identify bifurcations in the behavior of Eq. (27) (i.e., where the number of its fixed points changes) and then use multiple separate, continuous functions to find associated fixed points. Figure 4(c) shows the dependence of these fixed points on the constant touchdown power α with the touchdown angle chosen as $\beta=26°$.

B. Parameter dependence and stability of fixed points

Figures 5(a) and 5(b) respectively illustrate the apex height and apex energy fixed points of uncontrolled TD-SLIP locomotion as a function of both the constant touchdown angle $\beta \in [20°, 32°]$ and the constant touchdown power $\alpha \in [0.5, 2.5]$, computed using the procedure described above. The system generally has a single fixed point, except a narrow parameter range where there are two stable and one unstable fixed points, also shown on Fig. 4(c). Fixed points also become unstable once the choice of touchdown angle β becomes either too large or too small, as illustrated by the dark green regions in Fig. 5.
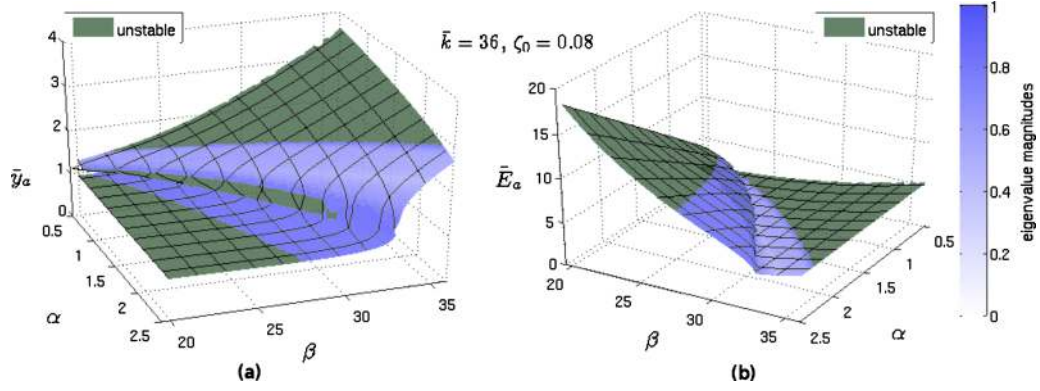
FIG. 5. (Color online) Dependence of (a) apex height and (b) apex energy fixed points and their stability for the uncontrolled TD-SLIP model on the constant touchdown angle β and touchdown power α parameters. Dark regions to the sides are unstable whereas light regions in the middle are stable with the shading intensity corresponding to the maximum eigenvalue magnitude as shown by the scale to the right.

In order to characterize the stability of fixed points, we have computed the eigenvalues of the associated Jacobian through analytic differentiation of the approximate return map described in Sec. II D. Figures 6(a) and 6(b) illustrate the behaviors of the eigenvalue with the maximum magnitude for two different settings of the touchdown angle as a function of the touchdown power α. The top plot clearly shows the presence of two saddle node bifurcations at the boundaries of the middle section with three fixed points. The left and right extremes of the top plot also show how the single point loses stability as the touchdown power goes outside the stable middle region. The bottom plot shows a touchdown angle setting where the region with three distinct fixed points is no longer observed.

The most important feature of these results, however, is the presence of two distinct regions for the stable fixed points. The first region, marked with (i) in Figs. 6(a) and 4(c), is robustly stable with the maximum eigenvalue well-below unity, but corresponds to very large apex heights (almost twice the leg length) that are not commonly observed

for biological or robotic systems. The second one, marked with (ii) in the same two figures, corresponds to much more realistic apex heights and speeds, but the associated eigenvalues are very close to unity, making the corresponding fixed points vulnerable to inaccuracies in our approximate map.

These observations are supported by the comparison of exact plant simulations to the predictions of our approximate map. Figure 7 shows the convergence behavior of a TD-SLIP system which started from different initial apex heights for different values of α and simulated for up to 150 strides. White regions in Fig. 7(a) correspond to structural locomotion failures such as toe-stubbing, failure to lift off, or reversal of locomotion direction. The large regions with the light shade correspond to simulations which did not converge within the 150 steps but did sustain locomotion. In contrast, regions with darker shades of blue correspond to initial conditions from which convergence to the fixed point associated with the corresponding choice of α was observed, with red dots indicating where the exact system converged to. As our approximations predicted, fixed points with large apex heights are robustly stable (despite the small discrepancy in the prediction of the actual fixed point location), whereas the practically feasible, lower apex height fixed points exhibit only marginal stability with an extremely small domain of attraction. These results show that practically, purely open-loop control of TD-SLIP locomotion is not very robust. In Sec. IV, we propose a novel energy-regulation scheme that partially preserves the open-loop nature of our control strategy with an uncontrolled leg placement angle, while substantially improving the robustness and stability of the resulting running behavior.

IV. STABILITY OF AN ENERGY-REGULATED TD-SLIP

A. Compensation of damping losses

In this section, we describe a new method to use the hip torque to compensate for all dissipative effects within a single step, ensuring conservation of energy in the apex return map and hence reducing its dimension by one. Our con-
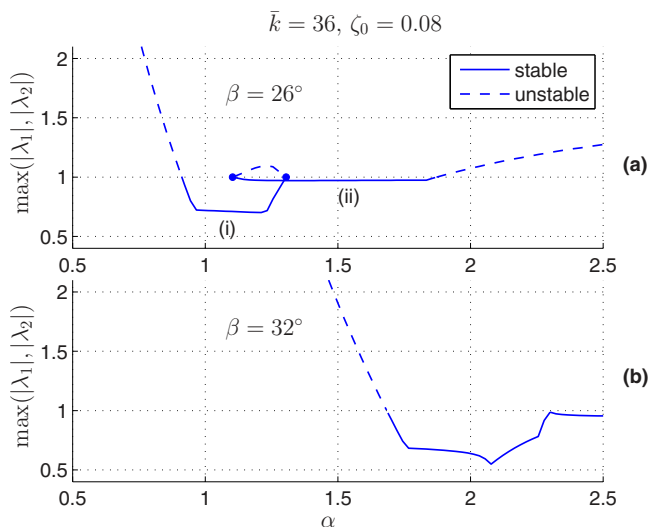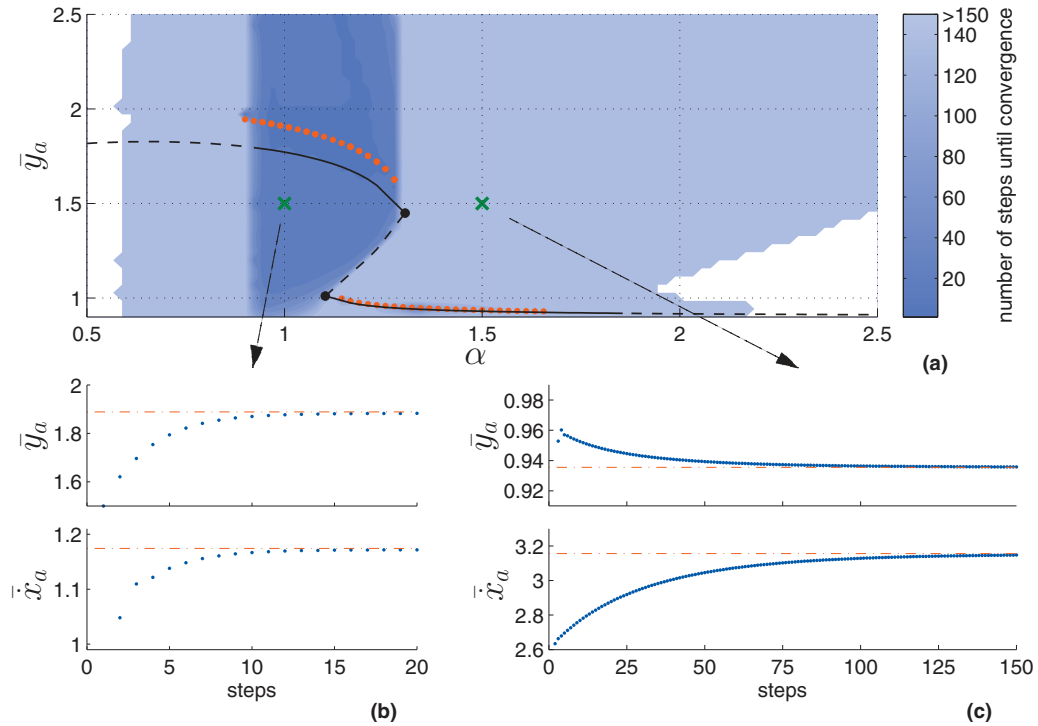

FIG. 6. (Color online) Maximum eigenvalue magnitudes for the analytically computed return map Jacobian evaluated at fixed points as a function of touchdown power for two different touchdown angles (a) $\beta=26°$ and (b) $\beta=32°$.

FIG. 7. (Color) (a) Comparison of fixed point behavior predicted by our analytic approximations to the exact TD-SLIP plant model for $\beta = 26°$. Black traces show predictions of our approximations, with dashed sections unstable, whereas red dots indicate where exact TD-SLIP simulations converge to. Dark shaded regions illustrate the basin of attraction for the simulated plant with lighter shades having larger convergence time. Initial conditions in white regions result in structural failure such as toe stubbing. Bottom: (b) fast and (c) slow convergence with $\alpha = 1$ and $\alpha = 1.5$, respectively, of numerical TD-SLIP simulations which started from initial conditions shown with green crosses in (a).

sideration of energy as a controlled variable is similar in spirit to previous passive stability experiments conducted on the ARL Monopod-II robot platform.[40]

Note that the total energy dissipated within a single TD-SLIP step is given by

$$E_{\text{loss}} = E_c + E_k, \tag{29}$$

where E_c represents damping losses with

$$E_c := \int_0^{t_{lo}} c\dot{r}^2(\eta)d\eta, \tag{30}$$

and $E_k := (r_{lo} - r_0)^2/2$ captures the leftover energy in the leg spring when it lifts off before it is fully extended due to damping. Fortunately, our analytic approximations provide closed form expressions for both of these components. In particular, damping losses can be approximately computed as

$$E_c = \frac{-c/M^2\hat{\omega}_0}{4\zeta}(\zeta\cos(2(\phi_1 + \phi_2) + \phi_3) + 1$$
$$- e^{-2\zeta\hat{\omega}_0 t_{lo}}(\zeta\cos(2\omega_d t_{lo} + 2(\phi_1 + \phi_2) + \phi_3) + 1)), \tag{31}$$

while E_k only depends on the previously computed r_{lo} and ϕ_1, ϕ_2 and ϕ_3 defined as in Sec. II C.

In contrast, the energy supplied by the hip torque is given by Eq. (25), for which our analytical approximations can also be used to obtain closed-form expressions. Since both Eqs. (29) and (25) can be obtained in closed form as a function of initial conditions and the choice of touchdown angle θ_{td}, we can find the desired torque magnitude τ_0 by solving

$$E_\tau = E_{\text{loss}}. \tag{32}$$

As noted above, this choice of torque results in successive apex states having the same energy, at least while working within our approximate apex return map. Naturally, additional corrections are needed to apply these ideas to the exact plant model since inaccuracies of our approximations would invalidate this conservation. Nevertheless, we use this active compensation regime to reduce the dimension of our analytic apex return map, allowing us to easily identify its equilibrium points and characterize their stability.

B. Equilibrium points with a fixed leg placement policy

In this section, we use our analytic approximations to identify and characterize the equilibrium points of the one-dimensional "energy-regulated" return map on the apex height y_a arising from the use of a fixed touchdown angle policy with $\theta_{td} = \beta$ and the energy-regulating hip torque described in Sec. IV A. Figure 8 shows two families of return maps for $\beta = 22°$ (top) and $\beta = 30°$ (bottom), together with the dependence of equilibrium points on the energy level of the system in the right plots. These results show that the TD-SLIP still exhibits asymptotically stable behavior under the fixed touchdown angle, energy-regulated regime, with the location of the equilibrium point depending on the chosen energy level. In contrast to the fully uncontrolled system, the range of fixed points obtained under the energy regulation corresponds to much more realistic apex states and exhibits strong stability, as shown by the associated eigenvalue mag-
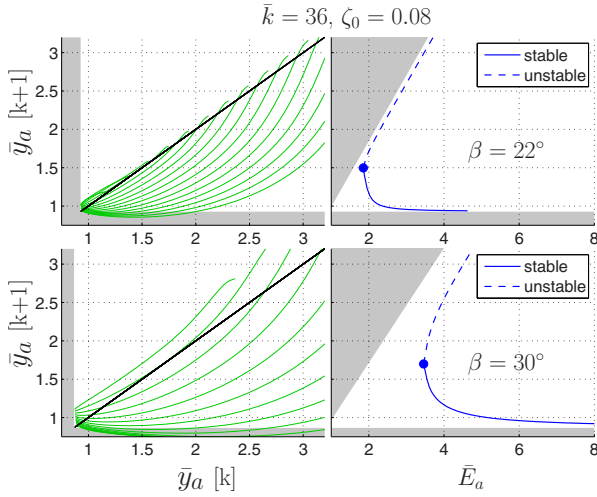
FIG. 8. (Color online) Apex height return map (left) and associated equilibrium points (right) for the TD-SLIP model with $\bar{k}=36$, $\zeta_0=0.08$, $\beta=22°$ (top), and $\beta=30°$ (bottom) plotted for different (dimensionless) apex energy levels in the range $\bar{E}_a \in [1,8]$, generated with the proposed analytical approximations. Shaded regions correspond to kinematically infeasible configurations.
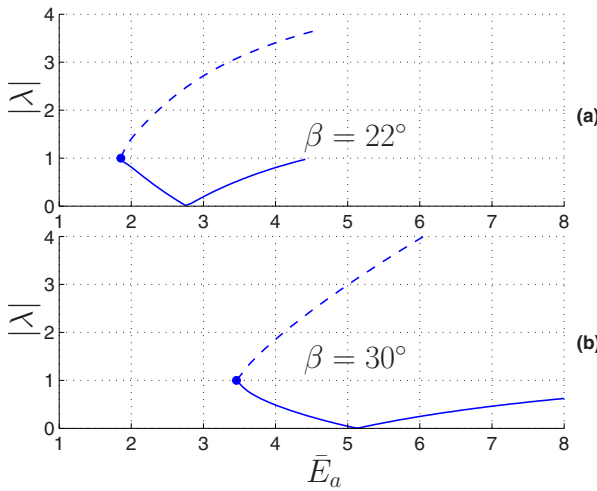

FIG. 9. (Color online) Numerically computed eigenvalues of stable and unstable fixed points for energy-compensated TD-SLIP locomotion with $\bar{k}=36$, $\zeta_0=0.08$ and (a) $\beta=22°$, and (b) $\beta=30°$.

nitudes in Fig. 9 and fast convergence times (at most eight steps for most initial conditions) observed in exact plant simulations of Fig. 10.

We can also observe that as the fixed touchdown angle β increases, the energy range for which stable fixed points exist increases as well. This is rather natural since the torque actuation at the hip can only supply energy through the angular momentum, which directly increases the angular span during stance. Increasing the touchdown angle admits a larger angular span for stance, allowing stable fixed points to form at higher energy levels as well.

Having established the presence of stable equilibrium points for the energy compensated TD-SLIP model, Fig. 10 shows a comparison of fixed points predicted by our analytic approximations with those that arise within simulations of the exact TD-SLIP model in apex height and apex speed coordinates. In order to make direct comparisons possible, we started TD-SLIP simulations from a large range of initial y_a and E_a values, with a fixed touchdown angle and an energy-regulation controller similar to the one presented in Sec. IV A, but now taking the energy level of the very first step as an overall regulation goal. This modification was necessary since using the approximations to locally enforce energy conservation at every step would slowly cause prediction errors to accumulate, either draining all energy out of the system, or causing it to diverge. We then checked whether the system converges to a stable equilibrium point in apex coordinates after 50 steps up to a tolerance of 10^{-4}. The blue regions in both plots illustrate the resulting domain of attraction with lighter shades having longer convergence times, while the red line in the same plot illustrates the associated set of fixed points.

The domain of attraction exhibited by the simulation almost exactly covers the region between the unstable and stable fixed points predicted by our approximations. There is also an almost exact match between the fixed points predicted by our approximations and those obtained from simulation except regions very close to the saddle node bifurcation at low energy levels. The cavities to the right of the region of attraction arise from the presence of the "gap" region in the return map, resulting from kinematic constraints
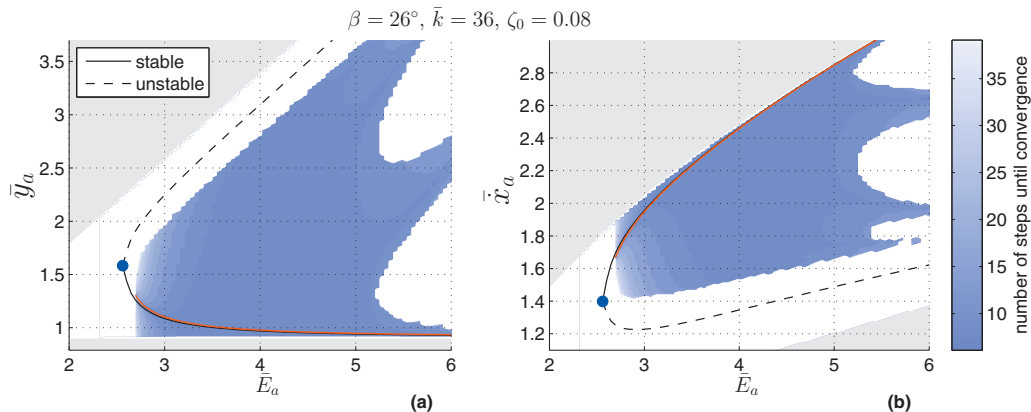

FIG. 10. (Color) Comparison of (a) stable apex height and (b) stable apex speed equilibrium points predicted by our analytic approximation (solid black line) with those obtained by exact plant simulations (red line) for $\beta=26°$ and different apex energy levels in the range $\bar{E}_a \in [2,6]$. Blue shaded regions illustrate stable domains of attraction for the simulated plant model.
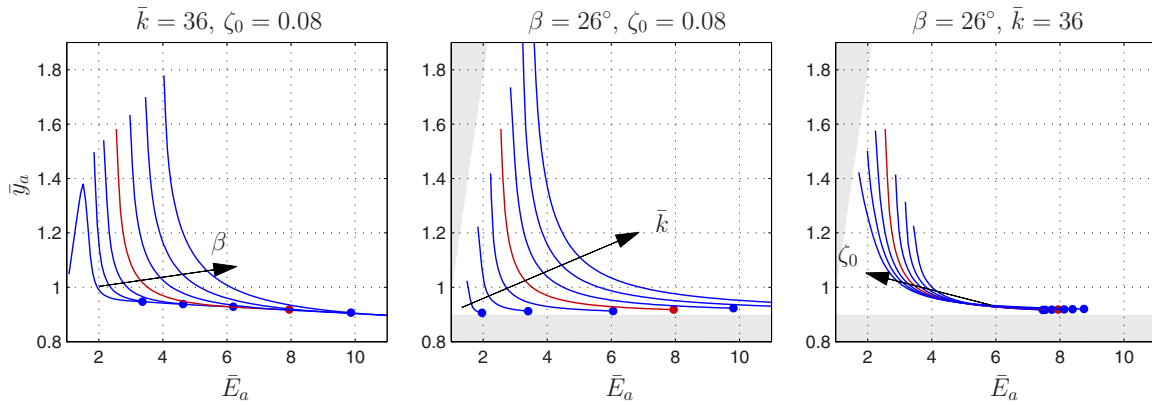
FIG. 11. (Color online) Dependence of stable equilibrium points on variations of the touchdown angle β (left), leg spring stiffness $\bar{k}$ (middle), and leg damping ratio ζ_0 (right). Arrows indicate increasing directions for each varied parameter and small circles mark the end points of each curve for clarity.

that require the apex height to be sufficiently large to allow leg placement. The reason for this can be clearly seen in both right plots of Fig. 8, where parts of the return map overlap with the kinematically infeasible gray region on the bottom. This means that some initial conditions at high energy levels will lead to apex states for which leg placement at an angle of β is impossible. This gap was also observed by previous studies,[26] and is reproduced by both our analytical approximations, and the simulated plant. Finally, we also note that apex speeds associated with the fixed points of the system are physically realistic ($\bar{x}_a = 1.5$ corresponds to roughly $\dot{x}_a = 4.7$ m/s for an average sized human) and both coordinates in the apex return map are accurately predicted by our approximations.

C. Parameter dependence of equilibrium points

Equilibrium points that arise from our fixed touchdown angle, energy-regulated regime naturally depend on the kinematic and dynamic parameter choices. Figure 11 illustrates the dependence of stable fixed points on each individual parameter (the touchdown angle β, the dimensionless leg stiffness $\bar{k}$, or leg damping ζ_0) with the remaining two parameters kept constant. Compatible with our observations of Sec. IV B, the range of stable energy levels increases with larger touchdown angles (i.e., for $\beta = 20°$, $\bar{E}_a \in [1.1, 3.4]$

whereas for $\beta = 30°$, $\bar{E}_a \in [3.45, 11.9]$), as illustrated by Fig. 11, where we marked the end points of each curve with a small circle for visibility.

The dependence of equilibrium points on the leg stiffness, illustrated in the middle figure, shows that increasing spring constants cause an increase in the range of stable energy levels. This is also natural since an increased stiffness corresponds to shorter stance times, resulting in decreased damping losses and a corresponding decrease in the necessary torque input. Finally, we observe that the impact of the damping coefficients on the equilibrium points is not as pronounced, providing evidence that our compensation strategy successfully balances damping losses. Nevertheless, increasing the amount of damping causes a slight decrease in the range of stable energy levels.

D. Correspondence of the model to biological data

A recent quantitative comparison of ground reaction force data from a variety of running animals to those predicted by a simple, passive spring-mass model shows that despite the very good correspondence of vertical force components between biological data and the idealized SLIP model, there are some discrepancies in how well horizontal forces can be predicted.[53] In this section, we report on an interesting property of the torque-actuated TD-SLIP mor-
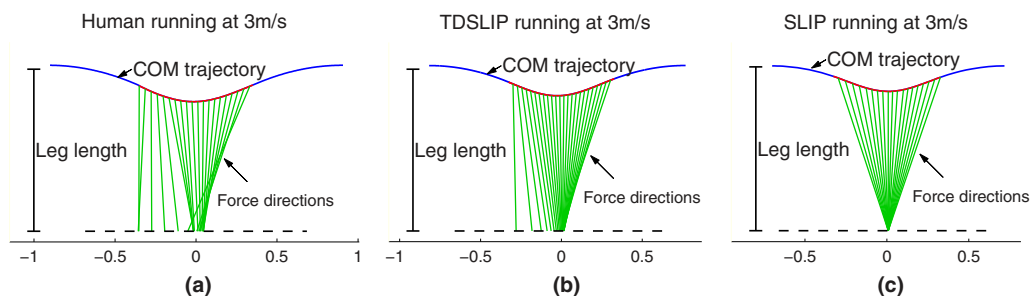

FIG. 12. (Color online) Center-of-mass trajectories and directions of stance ground reaction forces of (a) human running, (b) TD-SLIP running, and (c) SLIP running at approximately 3 m/s across a single stride with $m = 65.4$ kg and $r_0 = 1$ m. Data for the left plot were extracted from Kram and Griffin (Ref. 54), while the middle and right plots were obtained using TD-SLIP and SLIP simulations, respectively. Lightly shaded lines in all plots show the directions of ground reaction forces during stance as in Srinivasan and Holmes (Ref. 53).

phology: it seems to be capable of qualitatively reproducing ground reaction force profiles very similar to those observed in biological systems.

Figure 12 illustrates body COM trajectories for a single stride of steady-state running for (a) human running, (b) running with the TD-SLIP model, and (c) running with the conservative SLIP model, together with a depiction of "virtual footfalls" in the direction of instantaneous ground reaction force vectors throughout the stance phase as proposed by Srinivasan and Holmes.[53] COM trajectories associated with human running were extracted from ground reaction force data in Kram and Griffin[54] through integration and filtering by assuming periodicity of motion in both position and velocity variables together with the average locomotion velocity, standard techniques in biomechanics for recovering positional trajectories from force-plate measurements. Dynamic parameters for both the TD-SLIP and SLIP data in the middle and right figures were manually tuned to obtain COM trajectories and an average locomotion speed close to those associated with human data.

The commonly used lossless SLIP model was previously found to be incapable of capturing the backward bias in the horizontal ground reaction forces observed in human running data.[53] However, as a result of the ramp torque profile we use for supplying energy to the system, TD-SLIP locomotion does result in large backward horizontal forces introduced in the beginning of the stance phase, with associated virtual footfalls appearing behind the actual toe location. Toward the end of the stance phase, the hip torque approaches zero and brings the virtual footfall and actual toe locations together. This qualitative structure is observed for all steady-state trajectories of the TD-SLIP model and is remarkably consistent with data from human locomotion. Even though we do not yet have any quantitative basis in which any predictive claims can be made, we think that this correspondence may provide evidence toward both the presence of significant damping, and the use of hip torque as an additional source of energy used by biological runners, improving the predictive accuracy and utility of dynamic models of running.

V. APPLICATION: FEEDBACK CONTROL OF TD-SLIP RUNNING

A. Deadbeat control by inversion of the apex return map

The presence of a sufficiently accurate analytic formulation of the apex return map naturally motivates its inversion to obtain a controller for actively stabilizing the system around a desired operating point $[y_a^*, \dot{x}_a^*]$ in apex state coordinates. A similar approach was adopted in a number of studies,[22,33,55] but never in the context of a lossy model or torque actuation. In this section, we describe a deadbeat gait controller for TD-SLIP as an application of our approximations, and show that it is capable of very accurately regulating the apex states of a running TD-SLIP and improves on both the accuracy and stability of previous attempts to control a similar, torque-actuated model.[36]

An explicitly specified desired apex state will require a nonzero change in the energy level of the system. Using a strategy similar to the energy-conserving torque controller of Sec. IV A, we will use the hip torque to supply the requested energy input to the system in a single step. Similar to Eq. (32), this energy is given by

$$E_\tau = \frac{1}{2}m((\dot{x}_a^*)^2 - \dot{x}_a^2) + mg(y_a^* - y_a) + E_{\text{loss}}, \tag{33}$$

which can easily be solved to determine the ramp torque magnitude τ_0, assuming, once again, that $t_f = t_{lo}$.

Once the desired torque profile is determined, the return map has only one remaining degree of control freedom: the touchdown angle θ_{td}, no longer kept constant across subsequent strides. A deadbeat controller can be formulated as a one-dimensional minimization problem in the form

$$\theta_{td} = \underset{-\pi/2 < \theta < -\pi/2}{\text{argmin}} (\dot{x}_a^* - (\pi_{\dot{x}_a} \circ P(\theta_{td}, [y_a, \dot{x}_a]_k)))^2, \tag{34}$$

whose numerical solution is trivial due to the availability of our analytic approximation for the return map P. This yields an effective, one-step deadbeat controller for the regulation of forward speed and hopping height for the TD-SLIP model.

B. Controller performance and comparison

As noted before, there are very few in depth studies of how hip torque actuation can be used to achieve stable locomotion. Among notable exceptions is recent work on locomotion over mildly rough terrain[36] where the authors use TD-SLIP equations of motion to derive an approximate energy controller to regulate hopping height, and a proportional-derivative (PD) torque policy to regulate forward speed. In this section, we present a comparison of this controller with the new controller we described in Sec. V A. In order to maintain consistency with our previous stability results, we use the same kinematic and dynamic parameters with Sec. IV B, roughly corresponding to an average human morphology. Note that parameters used by Papadopoulos et al.[36] were also not substantially different from ours when converted to dimensionless units. All simulations were run in MATLAB using a fourth order Runge–Kutta integrator together with accurate detection of transition events. Each run consisted of 50 steps, at the end of which we determined whether there was convergence to a fixed point in apex coordinates.

Figure 13 illustrates tracking performances of both controllers for apex speed and height variables in terms of normalized percentage error measures. Note that our controller based on an accurate analytic model for the dynamics of TD-SLIP significantly increases the range of velocity goals that can be achieved without losing stability. Moreover, improvements can be observed in the tracking accuracy for both the apex speed and height variables. Finally, our controller does not require any feedback or sensory measurements during stance, but relies only on accurate measurement of apex states. This makes practical implementations much more feasible compared to the active PD control strategy since high-bandwidth feedback is usually very challenging for fast legged robots.
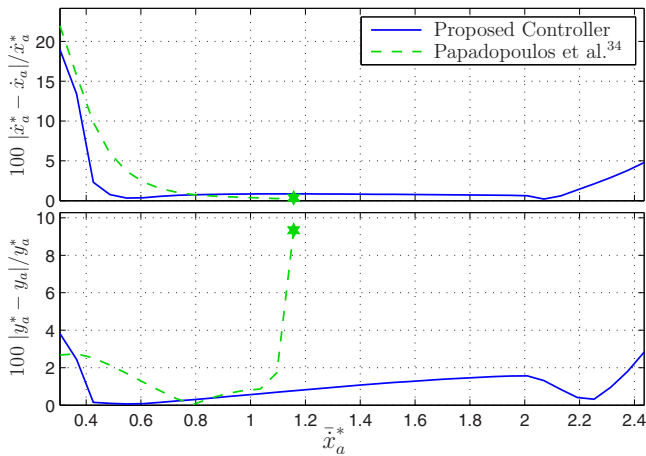
FIG. 13. (Color online) Comparison of performance through percentage tracking errors for apex speed (top) and apex height (bottom) between the proposed controller [solid (blue)] and the PD control policy by Papadopoulos *et al.* (Ref. 36) [dashed (green)] as a function of (dimensionless) desired velocity $\bar{\dot{x}}_a^*$. Markers indicate where the controller of Ref. 36 loses stability. Vertical axes are percentage errors.

VI. CONCLUSION

In this paper, we presented a novel method to obtain analytical approximations to the stance trajectories of a dissipative, torque actuated planar spring-mass hopper. We have successfully used our approximations to first investigate stability properties of uncontrolled locomotion with this system with both the touchdown angle and stance torque profile control inputs kept constant across all strides. We established that the uncontrolled system possesses self-stabilizing limit cycles across a large range of parameter settings, but observed that those that correspond to physically realistic gaits have only marginal stability with very small domains of attraction and hence may not persist in the presence of modeling noise.

Subsequently, we proposed an energy-regulation controller for the hip torque that can accurately compensate for the effects of damping within a stride, allowing us to obtain a one-dimensional return map under a fixed angle leg placement policy, also substantially improving on the stability of resulting limit cycles. Once again, we were able to use our approximations to analyze stability properties of the model under this new energy-regulation scheme, identifying and characterizing its equilibrium points. The predictive accuracy of our analytical approximations was confirmed by a very close match to fixed points and their domains of attraction obtained through numerical simulations of the exact plant model. We have also demonstrated the utility of our approximations through their use in designing a gait controller.

It is important to note that neither the energy regulating hip torque controller nor the subsequent stability analysis would have been possible in the absence of our analytical approximations. Consequently, we believe this paper presents the first careful study of stability properties of running in the presence of non-negligible damping and hip torque actuation. In this context, we believe that the incorporation of damping as a significant component in the dynamical model substantially increases the applicability of associated analytical tools and controllers to practical robot platforms in which dissipative effects will always be present and may sometimes be a dominant factor particularly if compliance is achieved through composite materials. In the future, we hope to demonstrate the practical utility of our approximations by experimental verification of their predictions with respect to a physical monopedal runner.

Our choice of hip torque as the primary source of energy input to the system was motivated by the difficulty of implementing radial actuation in physical robot platforms, and the simplicity and success of existing robot platforms with similar actuation mechanisms.[1,5] We have also further simplified our model by assuming a fixed body angle that may be justified by morphologies in which additional legs on the front and back of the body provide a stabilizing effect, or where the body link is explicitly constrained by an experimental setup.[35,36] In this context, we discovered an interesting correspondence between the ground reaction force profiles resulting from the use of a hip torque and biological data presented in Ref. 53, leading to a possible explanation for the inability of the original SLIP model in reproducing horizontal force components during running and a very preliminary hypothesis that hip torque may be playing a previously unaddressed important role in the control of legged locomotion. In the future, we hope to generalize our results to a freely rotating body link, making the results applicable to less constrained morphologies such as bipeds. For example, one of the interesting possibilities is how forward-bending body posture and the resulting gravitational torque can be used to balance the torque input from the hip, making it possible to both have a freely rotating body, while using the hip torque to provide thrust. This seems to be one of the ways in which ideas similar to those used for passive dynamic walking can be applied to efficient bipedal running and we hope to extend our results in this paper to such scenarios.

[1]U. Saranli, M. Buehler, and D. E. Koditschek, "RHex: A simple and highly mobile robot," Int. J. Robot. Res. **20**, 616 (2001).
[2]J. G. Cham, S. A. Bailey, J. E. Clark, R. J. Full, and M. R. Cutkosky, "Fast and robust: Hexapedal robots via shape deposition manufacturing," Int. J. Robot. Res. **21**, 869 (2002).
[3]R. Playter, M. Buehler, and M. Raibert, "BigDog," in Society of Photo-Optical Instrumentation Engineers (SPIE) Conference Series, 2006, Vol. 6230.
[4]M. J. Spenko, G. C. Haynes, J. A. Saunders, M. R. Cutkosky, A. A. Rizzi, R. J. Full, and D. E. Koditschek, "Biologically inspired climbing with a hexapedal robot," J. Field Robot. **25**, 223 (2008).
[5]I. Poulakakis, J. A. Smith, and M. Buehler, "Modeling and experiments of untethered quadrupedal running with a bounding gait: The Scout II robot," Int. J. Robot. Res. **24**, 239 (2005).
[6]T. McGeer, "Passive dynamic walking," Int. J. Robot. Res. **9**, 62 (1990).
[7]M. Garcia, A. Chatterjee, A. Ruina, and M. Coleman, "The simplest walking model: Stability, complexity, and scaling," J. Biomech. Eng. **120**, 281 (1998).
[8]A. D. Kuo, "Stabilization of lateral motion in passive dynamic walking," Int. J. Robot. Res. **18**, 917 (1999).

[9]E. Westervelt, J. Grizzle, and D. Koditschek, "Hybrid zero dynamics of planar biped walkers," IEEE Trans. Autom. Control **48**, 42 (2003).

[10]S. Collins, A. Ruina, R. Tedrake, and M. Wisse, "Efficient bipedal robots based on passive-dynamic walkers," Science **307**, 1082 (2005).

[11]P. Holmes, R. J. Full, D. E. Koditschek, and J. Guckenheimer, "The dynamics of legged locomotion: Models, analyses, and challenges," SIAM Rev. **48**, 207 (2006).

[12]M. Vukobratović and B. Borovac, "Zero-moment point-thirty five years of its life," Int. J. Humanoid Rob. **1**, 157 (2004).

[13]G. A. Cavagna, F. P. Saibene, and R. Margaria, "Mechanical work in running," J. Appl. Physiol. **19**, 249 (1964).

[14]R. Blickhan, "The spring-mass model for running and hopping," J. Biomech. **22**, 1217 (1989).

[15]T. A. McMahon and G. C. Cheng, "The mechanics of running: How does stiffness couple with speed," J. Biomech. **23**, 65 (1990).

[16]R. Blickhan and R. J. Full, "Similarity in multilegged locomotion: Bouncing like a monopod," J. Comp. Physiol., A **173**, 509 (1993).

[17]R. M. N. Alexander, *Principles of Legged Locomotion* (Princeton University Press, Princeton, NJ, 2006).

[18]D. E. Koditschek and M. Buehler, "Analysis of a simplified hopping robot," Int. J. Robot. Res. **10**, 587 (1991).

[19]W. J. Schwind, "Spring loaded inverted pendulum running: A plant model," Ph.D. thesis, University of Michigan, 1998.

[20]M. Raibert, *Legged Robots That Balance*, MIT Press Series in Artificial Intelligence (MIT, Boston, 1986).

[21]P. Gregorio, M. Ahmadi, and M. Buehler, "Design, control, and energetics of an electrically actuated legged robot," IEEE Trans. Syst., Man, Cybern., Part B: Cybern. **27**, 626 (1997).

[22]U. Saranli, "Dynamic locomotion with a hexapod robot," Ph.D. thesis, The University of Michigan, 2002.

[23]I. Poulakakis and J. W. Grizzle, "The spring loaded inverted pendulum as the hybrid zero dynamics of an asymmetric hopper," IEEE Trans. Autom. Control **54**, 1779 (2009).

[24]M. M. Ankarali, O. Arslan, and U. Saranli, "An analytical solution to the stance dynamics of passive spring-loaded inverted pendulum with damping," in 12th International Conference on Climbing and Walking Robots and the Support Technologies for Mobile Machines (CLAWAR'09), Istanbul, Turkey, 2009.

[25]W. J. Schwind and D. E. Koditschek, "Approximating the stance map of a 2-dof monoped runner," J. Nonlinear Sci. **10**, 533 (2000).

[26]H. Geyer, A. Seyfarth, and R. Blickhan, "Spring-mass running: simple approximate solution and application to gait stability," J. Theor. Biol. **232**, 315 (2005).

[27]J. J. Robilliard and A. M. Wilson, "Prediction of kinetics and kinematics of running animals using an analytical approximation to the planar spring-mass system," J. Exp. Biol. **208**, 4377 (2005).

[28]O. Arslan, U. Saranli, and O. Morgul, "An approximate stance map of the spring mass hopper with gravity correction for nonsymmetric locomotions," in Proceedings of the IEEE International Conference on Robotics and Automation, Kobe, Japan, 2009.

[29]R. Altendorfer, D. E. Koditschek, and P. Holmes, "Stability analysis of legged locomotion models by symmetry-factored return maps," Int. J. Robot. Res. **23**, 979 (2004).

[30]R. Altendorfer, D. E. Koditschek, and P. Holmes, "Stability analysis of a clock-driven rigid-body SLIP model for RHex," Int. J. Robot. Res. **23**, 1001 (2004).

[31]R. M. Ghigliazza, R. Altendorfer, P. Holmes, and D. Koditschek, "A simply stabilized running model," SIAM J. Appl. Dyn. Syst. **2**, 187 (2003).

[32]J. Schmitt, "A simple stabilizing control for sagittal plane locomotion," J. Comput. Nonlinear Dyn. **1**, 348 (2006).

[33]S. G. Carver, N. J. Cowan, and J. M. Guckenheimer, "Lateral stability of the spring-mass hopper suggests a two-step control strategy for running," Chaos **19**, 026106 (2009).

[34]H. Geyer, A. Seyfarth, and R. Blickhan, "Compliant leg behaviour explains basic dynamics of walking and running," Proc. R. Soc. London, Ser. B **273**, 2861 (2006).

[35]A. Sato and M. Buehler, "A planar hopping robot with one actuator: design, simulation, and experimental results," in Proceedings of the IEEE/RSJ International Conference on Intelligent Robots and Systems, 2004, Vol. 4, pp. 3540–3545.

[36]N. Cherouvim and E. Papadopoulos, "Control of hopping speed and height over unknown rough terrain using a single actuator," in Proceedings of the IEEE International Conference on Robotics and Automation, Kobe, Japan, 2009.

[37]R. J. Full and D. E. Koditschek, "Templates and anchors: Neuromechanical hypotheses of legged locomotion," J. Exp. Biol. **202**, 3325 (1999).

[38]M. Ankarali, U. Saranli, and A. Saranli, "Control of underactuated planar hexapedal pronking through a dynamically embedded slip monopod," in Proceedings of the International Conference on Robotics and Automation, Anchorage, Alaska, 2010.

[39]G. Zeglin, "The bow leg hopping robot," Ph.D. thesis, Carnegie Mellon University, 1999.

[40]M. Ahmadi and M. Buehler, "Controlled passive dynamic running experiments with the arl-monopod ii," IEEE Trans. Rob. **22**, 974 (2006).

[41]M. Wisse, D. G. E. Hobbelen, and A. L. Schwab, "Adding an upper body to passive dynamic walking robots by means of a bisecting hop mechanism," IEEE Trans. Rob. **23**, 112 (2007).

[42]T. Narukawa, M. Takahashi, and K. Yoshida, "Level-ground walk based on passive dynamic walking for a biped robot with torso," 2007 IEEE International Conference on Robotics and Automation, 2007, pp. 3224–3229.

[43]C. Chevallereau, E. R. Westervelt, and J. W. Grizzle, "Asymptotically stable running for a five-link, four-actuator, planar bipedal robot," Int. J. Robot. Res. **24**, 431 (2005).

[44]J. Seipel and P. Holmes, "A simple model for clock-actuated legged locomotion," Regular Chaotic Dyn. **12**, 502 (2007).

[45]N. Cherouvim and E. Papadopoulos, "Speed and height control for a special class of running quadruped robots," in Proceedings of the IEEE International Conference on Robotics and Automation, 2008, pp. 825–830.

[46]K. J. Waldron, J. Estremera, P. J. Csonka, and S. P. N. Singh, "Analyzing bounding and galloping using simple models," J. Mech. Rob. **1**, 011002 (2009).

[47]J. W. Hurst, J. E. Chestnutt, and A. A. Rizzi, "Design and philosophy of the bimase, a highly dynamic biped," in Proceedings of the International Conference on Robotics and Automation, 2007, pp. 1863–1868.

[48]A. D. Kuo, "Energetics of actively powered locomotion using the simplest walking model," J. Biomech. Eng. **124**, 113 (2002).

[49]D. I. Jindrich and R. J. Full, "Many-legged maneuverability: Dynamics of turning in hexapods," J. Exp. Biol. **202**, 1603 (1999).

[50]K. D. Mombaur, R. W. Longman, H. G. Bock, and J. P. Schloder, "Stable one-legged hopping without feedback and with a point foot," in Proceedings of the IEEE International Conference on Robotics and Automation, 2002, Vol. 4, pp. 3978–3983.

[51]A. Seyfarth, H. Geyer, and H. Herr, "Swing-leg retraction: a simple control model for stable running," J. Exp. Biol. **206**, 2547 (2003).

[52]R. M. Ghigliazza, R. Altendorfer, P. Holmes, and D. E. Koditschek, "A simply stabilized running model," SIAM Rev. **47**, 519 (2005).

[53]M. Srinivasan and P. Holmes, "How well can spring-mass-like telescoping leg models fit multi-pedal sagittal-plane locomotion data?," J. Theor. Biol. **255**, 1 (2008).

[54]R. Kram, T. M. Griffin, J. M. Donelan, and Y. H. Chang, "Force treadmill for measuring vertical and horizontal ground reaction forces," J. Appl. Physiol. **85**, 764 (1998).

[55]U. Saranli, W. J. Schwind, and D. E. Koditschek, "Toward the control of a multi-jointed monoped runner," in Proceedings of the IEEE International Conference on Robotics and Automation, New York, 1998, Vol. 3, pp. 2676–2682.